Journal of Applied Polymer Science

Phenolic resin-crosslinked natural rubber/clay nanocomposites: Influence of clay loading and interfacial adhesion on strain-induced crystallization behavior

Abdulhakim Masa,[1] Ryota Saito,[2] Hiromu Saito,[2] Tadamoto Sakai,[3] Azizon Kaesaman,[1] Natinee Lopattananon[1]

[1]Department of Rubber Technology and Polymer Science, Faculty of Science and Technology, Prince of Songkla University, Pattani 94000, Thailand

[2]Department of Organic & Polymer Materials Chemistry, Tokyo University of Agriculture and Technology, Koganei-Shi, Tokyo 184-8588, Japan

[3]Shizuoka University, Tokyo Office, Campus Innovation Center Tokyo, 3-3-6 Shibaura, Minato, Tokyo, 108-0023, Japan

Correspondence to: N. Lopattananon (E-mail: natinee.l@psu.ac.th) or H. Saito (E-mail: hsaitou@cc.tuat.ac.jp)

ABSTRACT: Nanocomposites of natural rubber (NR) and pristine clay (clay) were prepared by latex mixing, then crosslinked with phenolic resin (PhOH). For comparative study, the PhOH-crosslinked neat NR was also prepared. Influence of clay loading (i.e., 1, 3, 5, and 10 phr) on mechanical properties and structural change of PhOH-crosslinked NR/clay nanocomposites was studied through X-ray diffraction (XRD), transmission electron microscopic (TEM), wide-angle X-ray diffraction (WAXD), tensile property measurement, and Fourier transform infrared spectroscopy (FTIR). XRD and TEM showed that the clay was partly intercalated and aggregated, and that the dispersion state of clay was non-uniform at higher clay loading (>5 phr). From tensile test measurement, it was found that the pronounced upturn of tensile stress was observed when the clay loading was increased and a maximum tensile strength of the PhOH-crosslinked NR/clay nanocomposites was obtained at 5 phr clay. WAXD observations showed that an increased addition of clay induced more orientation and alignment of NR chains, thereby lowering onset strain of strain-induced crystallization and promoting crystallinity of the NR matrix during tensile deformation. FTIR investigation indicated a strong interfacial adhesion between NR matrix and clay filler through a phenolic resin bridge. This suggested that the PhOH did not only act as curative agent for crosslinking of NR, but it also worked as coupling agent for promoting interfacial reaction between NR and clay. The presence of strong interfacial adhesion was found to play an important role in the crystallization process, leading to promotion of mechanical properties of the PhOH-crosslinked NR/clay nanocomposites. © 2015 Wiley Periodicals, Inc. J. Appl. Polym. Sci. **2016**, *133*, 43214.

KEYWORDS: composites; crystallization; morphology; rubber; X-ray

Received 9 September 2015; accepted 10 November 2015
DOI: 10.1002/app.43214

INTRODUCTION

Natural rubber (NR) is one of the most widely used materials for industrial and household applications.[1] However, NR is rarely applied in its pure form as it is too weak to fulfill practical application requirements because of lack of hardness, strength properties, and wear resistance.[2] Practically, a common approach for mechanical property enhancement of NR is accomplished by introduction of chemical curative agents and reinforcing fillers.

Nowadays, NR nanocomposites reinforced by nanoclay have received a great deal of attention in rubber research area and industry due to the potential to improve mechanical properties, heat and oil resistance, and gas barrier properties, even by only small amounts of the clay.[3] Since, it has been well established that the excellent mechanical property of NR has been attributed to strain-induced crystallization.[4,5] The strain-induced crystallization in the crosslinked neat NR was thought to originate from the stretched crosslinked network structure.[4,6] Upon inclusion of nanoclay, the strain-induced crystallization of crosslinked NR under deformation was quite different from the crosslinked pure one because the microstructure of NR was remarkably changed.[7–10] In general, the ability to crystallize crosslinked NR nanocomposites was accelerated and the rate of crystallization was increased by the dispersed clay. In the popular model of strain-induced crystallization for NR/clay nanocomposites proposed by Carretero-Gonzalez *et al.*,[7,8] the strain-induced crystallization of crosslinked NR under extension was

enhanced because of clay orientation at low level of strain (<300%), followed by crystallization of network NR chains at high level of strain (>300%). As a consequence, the onset of strain-induced crystallization of NR/clay nanocomposites started at lower strain, and the rate of crystallization was greater upon stretching when compared with the neat crosslinked NR. Recently, Masa *et al.*[11] have developed the NR/pristine clay nanocomposites with a much higher level of mechanical property improvement when compared with the neat NR through the use of phenolic resin (PhOH) as curative agent and fixed clay loading (5 phr). The reinforcement mechanism of the PhOH-crosslinked NR nanocomposites was also proposed. The strain-induced crystallization of the PhOH-crosslinked NR nanocomposite was thought to associate with a preferred alignment of NR chains induced by clay rotation in the stretching direction at low strain level (<300%), and subsequently induced by collaborative activity of clay and crosslinking points at high strain level (>300%). In this mechanism, it was assumed that the NR chains were linked to the clay surface through a strong interfacial interaction between the NR matrix and clay; i.e., specific interaction between NR and clay and intercalation of NR chain in between clay galleries, which favored the strain-induced crystallization of nanocomposites. However, the detailed understanding of the interfacial interaction between NR and clay is lacking in the proposed model, and the effect of such interaction on strain-induced crystallization is not described.

For the rubber/clay nanocomposites, the mechanical properties and the strain-induced crystallization of rubber showed a strong dependence on clay loading.[12–16] Wang *et al.*[12,13] studied the mechanical properties and strain-induced crystallization of the rectorite and modified-montmorillonite clay filled NR nanocomposites with different clay loadings. They reported that the tensile stress for the crosslinked NR nanocomposites during stretching increased with increasing clay loading, whereas the best tensile strength was obtained at 5 phr clay. The decrease of tensile strength at higher clay loading (>10 phr) was related to the hindered strain-induced crystallization as analyzed through the stress–strain behavior of different NR nanocomposites. Later, Qu *et al.*[14] investigated the influence of organoclay loading on the mechanical properties and structure of NR/organoclay nanocomposite by using tensile test, Synchrotron 2-D wide-angle X-ray diffraction (WAXD), and transmission electron microscopic (TEM) techniques. The results showed the variations of tensile strength and degree of strain-induced crystallization with clay loading and clay dispersion. The maximum tensile strength was obtained at the clay content of 5 wt %, at which the crystalline content of NR reached a maximum. Similar observation was also reported for the NR/organoclay nanocomposites[15] and the isoprene rubber/organoclay nanocomposites.[16] However, from the above reports, their discussion is limited to sulfur and peroxide-crosslinked NR/clay nanocomposites. Therefore, it is necessary to explore the influence of clay loading on structure–property relationship for the PhOH-crosslinked NR/clay nanocomposites.

In this study, we prepared NR nanocomposites containing various amounts of pristine clay by using latex compounding method. PhOH was used to crosslink NR/clay nanocomposites. X-ray diffraction (XRD) and TEM were used to characterize the morphology of the NR nanocomposites. The mechanical properties and strain-induced crystallization were studied by using tensile test and WAXD measurements. Furthermore, the interfacial adhesion of the NR and pristine clay was investigated by Fourier transform infrared spectroscopy (FTIR). The role of interfacial adhesion on the crystallization process was discussed. Further, the reinforcement mechanism proposed by Masa *et al.*[11] was refined to better understand the strain-induced crystallization of NR/clay nanocomposites.

Table I. Formulation of Phenolic Resin-Crosslinked NR/Clay Nanocomposite (PhOH-NRNC)

Chemicals	Part per hundred parts of rubber (phr)
NR	100
Clay (Na-MMT)	0, 1, 3, 5 and 10
Phenolic resin (HRJ-10518)	10
Catalyst ($SnCl_2.2H_2O$)	1

EXPERIMENTAL

Materials

NR latex containing dry rubber content of 60% and stabilized with high concentration of ammonium was supplied by Yala Latex Co., Ltd. (Yala, Thailand). Unmodified clay used was sodium montmorillonite (Na-MMT, Kunipia-F®) which was kindly provided by Kunimine Industries Co., Ltd. (Tokyo, Japan). Hydroxymethylol phenolic resin (HRJ-10518) used as crosslinking agent was manufactured by Schenectady International Inc. (New York, US). The softening point and specific gravity of HRJ-10518 were 80–95°C and 1.05, respectively. Stannous chloride ($SnCl_2.2H_2O$) used as a catalyst for crosslinking reaction of phenolic resin was manufactured by Carlo Erba Reagent (Val de Reuil, France). It has melting point of 37°C and density of 2.71 g/cm^3.

Preparation of NR/Clay Nanocomposites

Suspension of clay in water (2 wt %) was prepared by dispersing clay in water with continuous stirring using IKA® RW 20 digital mixer (Germany) for 60 min at 1200 rpm. The clay suspension was then added into the NR latex. The NR/clay mixture was mixed under vigorous stirring (600 rpm) at ambient temperature for 30 min, and dried at 50°C for 3 days. The mixture was later compounded with phenolic resin (HRJ-10518) and catalyst ($SnCl_2{\cdot}2H_2O$) in a mixing chamber of a miniature mixing machine (IMC-18D7, Imoto Machinery Co., Ltd., Japan) at rotor speed of 140 rpm and temperature of 100°C for 20 min. The amounts of NR, clay, phenolic resin, and catalyst used in the preparation of nanocomposite compound are given in Table I. The compound was then melt pressed in a small hot-press machine (Imoto Machinery Co., Ltd., Japan) at 180°C to produce the PhOH-crosslinked NR/clay nanocomposite film with a thickness of 1 mm. The PhOH-crosslinked NR specimen without clay was also prepared by using the formulation given in the Table I and same procedure as described above. The PhOH-crosslinked NR/clay nanocomposites (PhOH-NRNCs) with four different clay loadings (1, 3, 5, and 10 phr) were abbreviated as

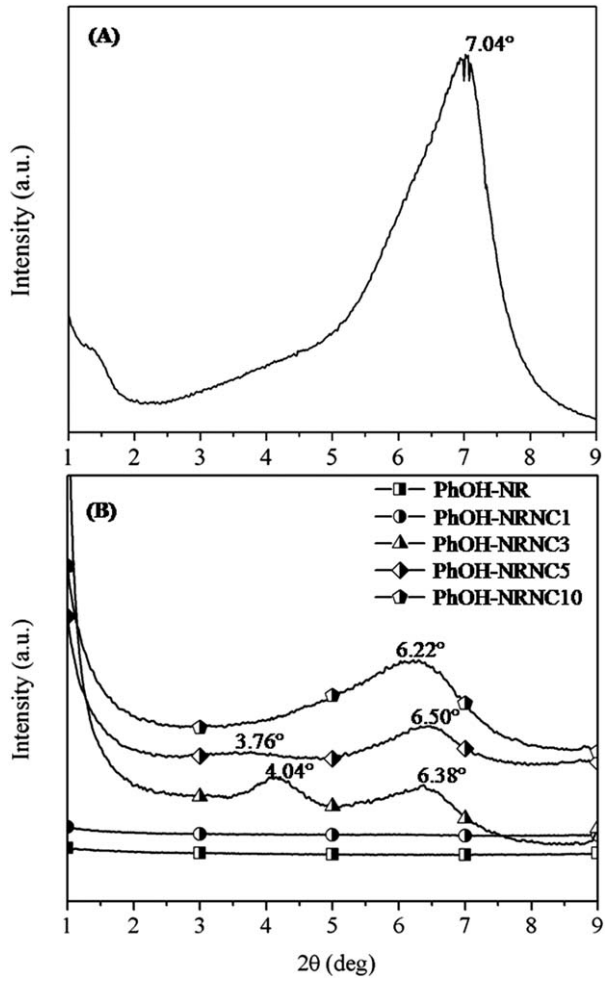

Figure 1. XRD patterns of (A) Na-MMT and (B) PhOH-NR and PhOH-NRNCs containing different clay loadings.

PhOH-NRNC1, PhOH-NRNC3, PhOH-NRNC5, and PhOH-NRNC10, respectively, whereas the PhOH-crosslinked NR without clay was abbreviated as PhOH-NR.

Characterizations

The *d*-spacing (d_{001}) of Na-MMT and PhOH-NRNCs was measured using XRD (Rigaku TTRAXII, Japan) analysis with Cu-Kα radiation of wavelength (λ) of 0.154 nm generated at voltage of 50 kV and current of 300 mA. The 2θ scanning of X-ray intensity was in the range of 1°–9° with a scanning rate of 1 °/min.

The dispersion of clay in the PhOH-NRNC samples was investigated by using TEM analysis. Ultra-thin section (ca. 100 nm) for TEM analysis was cut normal to the nanocomposite film plane with a diamond knife at −100°C. The sectioned samples were then observed by using JEOL JEM-2010 and JEM-2100 TEM (JEOL Co., Japan).

The mechanical properties were performed by using a tensile testing machine (StrographVES05D, Toyoseiki Co., Ltd., Japan) according to JIS K 6251. The samples were cut into a dumb-bell shape of 35 mm length. The samples were then stretched at room temperature with an extension rate of 200 mm/min. Five specimens were used for the tensile test.

The degree of crystallinity in the PhOH-NR and PhOH-NRNCs during tensile stretching was examined by using WAXD. The WAXD experiment was performed using NANO-Viewer system (Rigaku Co., Japan). A Cu-Kα radiation of wavelength of 0.154 nm was generated at 46 kV and 60 mA, and collimated by a confocal max-flux mirror system. The samples were stretched in steps during WAXD measurement at fixed strain using a miniature tensile machine (Imoto Machinery Co., Ltd., Japan). The exposure time was 15 min for WAXD measurement. All measurements were performed at room temperature (20°C). The scattering intensity was corrected with respect to the exposure time, the sample thickness, and the transmittance.

The interfacial interaction of PhOH-NRNC was studied by using Fourier transform infrared spectroscopy (FTIR) (JASCO FT/IR-4100, JASCO Corporation, Japan). The samples were compressed by using the small hot-press machine to obtain the thin film with a thickness of 50 μm. The FTIR spectra of the thin samples were recorded at room temperature in the range of 700–4000 cm^{-1}. The chemical structure of Na-MMT, PhOH, NR, and PhOH containing NR/clay compound or uncrosslinked NR/clay nanocomposite (PhOH-UNRNC) were also studied by FTIR technique.

RESULTS AND DISCUSSION

Dispersion of Clay

Figure 1 shows XRD patterns of Na-MMT, PhOH-NR, and PhOH-NRNCs with various clay loadings. The corresponding *d*-spacing (d_{001}) of these samples calculated by Bragg's equation ($d = \lambda/2 \sin \theta$) are presented in Table II. From Figure 1, it can be seen that the diffraction peak of pure clay appeared at 7.04°, which was related to the interlayer spacing (d_{001}) of 1.26 nm. It is also seen that there was no diffraction peak in the 2θ range of interest (1°–9°) for the PhOH-NR and the PhOH-NRNC1, while two different peaks were clearly observed at 2θ between 3.40° and 5.00° and 5.00° and 7.50° in the PhOH-NRNC3 and PhOH-NRNC5, except for the PhOH-NRNC10. Normally, the disappearance of any coherent XRD peak from the clay layers indicated the delaminated structure of clay.[17,18] However, in case of the PhOH-crosslinked NR filled with 1 phr clay (PhOH-NRNC1), the TEM study [shown in Figure 2(A,D)]) suggested that the delamination of clay into single platelet was not observed, while aggregations composed of several platelets (i.e., clay tactoid) existed in this sample. Upon increased addition of clay, diffractograms showed two interlayer distances (d_{001}) equal to about 1.36–1.38 nm and 2.18–2.35 nm in the PhOH-

Table II. 2θ at Diffraction Peak and Basal Spacing of Na-MMT, PhOH-NR, and PhOH-NRNCs Containing Different Clay Loadings

Sample	2θ (degree)	d_{001} (nm)
Na-MMT	7.04	1.26
PhOH-NR	–	–
PhOH-NRNC1	–	–
PhOH-NRNC3	4.04, 6.38	2.18, 1.38
PhOH-NRNC5	3.76, 6.50	2.35, 1.36
PhOH-NRNC10	6.22	1.42

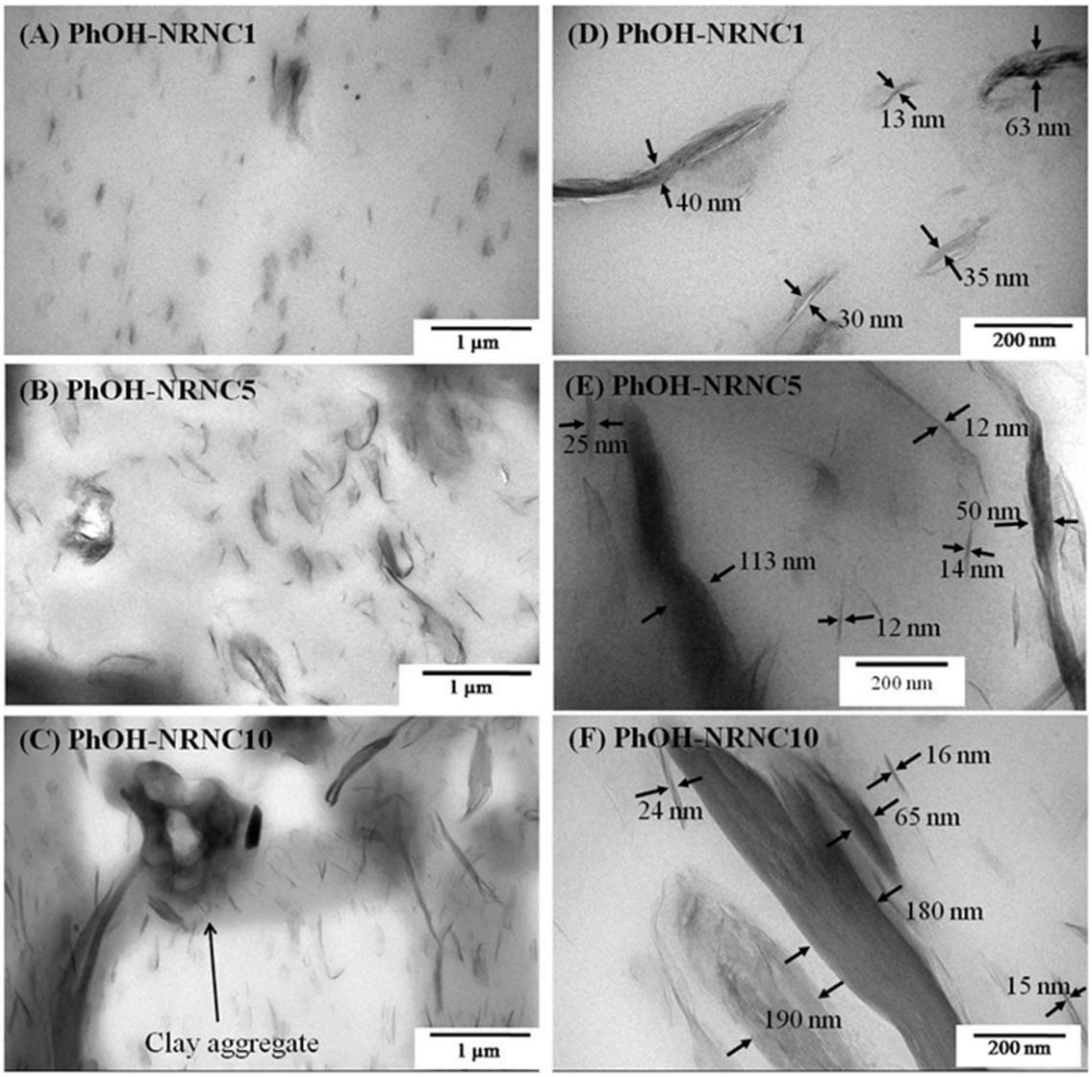

Figure 2. TEM images of PhOH-NRNCs containing different clay loadings at (A–C) low-magnification and (D–F) high-magnification.

crosslinked NR/clay nanocomposites with 3–5 phr clay (PhOH-NRNC3 and PhOH-NRNC5), while the PhOH-crosslinked NR/clay nanocomposite with 10 phr clay (PhOH-NRNC10) showed a single $d_{001} = 1.42$ nm. The increase in the interlayer spacing of clay in the nanocomposites compared to that in the original clay indicated that the clay layers were expanded due to insertion of rubber chain in the clay galleries, i.e., intercalated structure was formed.

So far, the TEM analysis is mainly used as a tool to visually compare the dispersion of clay layers.[19–21] Figure 2 shows TEM micrographs of thin section of PhOH-NRNCs containing 1, 5, and 10 phr clay. In these micrographs, the dark lines and lighter region represented the intersections of the clay layers and rubber matrix, respectively. In the PhOH-NRNC1, the clay tactoids were widely spread due to low filler content and the clay particles dispersed uniformly in the NR matrix [Figure 2(A)]. The size of clay tactoids was about 10–60 nm as shown in the enlargement in Figure 2(D). From Figure 2(B), the 5 phr clay nanocomposite (PhOH-NRNC5) still showed good clay dispersion, even though the size of clay tactoids was apparently larger (12–110 nm) [Figure 2 (E)] when compared with the nanocomposite containing 1 phr clay. With higher loading of 10 phr clay (PhOH-NRNC10), the clays were not well dispersed over the entire NR matrix [Figure 2(C)], and the aggregate size of clay was about 15–230 nm [Figure 2(F)]. The observation of XRD patterns coupled with the TEM images suggested that the clay was intercalated by rubber chains, and the clay layers were aggregated to form large tactoids in the NR matrix. Furthermore, the addition of significant amount of clay (10 phr) in the NR matrix probably resulted in poor dispersion of clay tactoids.

Tensile Properties

Figure 3 shows stress–strain curves of the PhOH-NR and PhOH-NRNCs containing different amounts of clay. The representative stress–strain curves of the PhOH-NR and PhOH-NRNCs exhibited a typical strain-induced crystallization behavior. That is, the initial stress slowly increased as a function of applied strain and when the strain reaches a certain value, the stress increases sharply, i.e. stress upturn due to strain-induced crystallization of NR during tensile process.[3,22] The stress upturn and the level of strain, at which the stress upturn

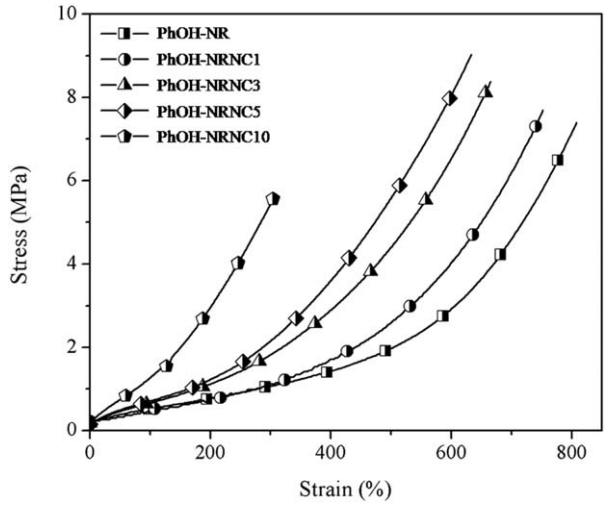

Figure 3. Stress–strain curves of PhOH-NR and PhOH-NRNCs containing different clay loadings.

started, appeared to be different in the NR with and without clay.

From the stress data of the stress–strain curves (Figure 3), it is possible to identify the turning point of strain by estimating derivative stress at various strains. Figure 4 shows the stress–strain curve coupled with derivative stress–strain curve for the PhOH-NR, as an example. When the applied strain exceeded the strain level of 495%, the estimated derivative stress abruptly increased with increasing strain. The first abrupt change in the derivative stress of the derivative stress–strain curve was identified as the onset of stress upturn. Based on this estimation, the values of strain at the onset of stress upturn for the PhOH-NRNCs and corresponding PhOH-NR were obtained as shown in Table III. It is obvious that the strain at the onset of stress upturn in the stress–strain curves for the PhOH-NRNCs was much lower than that of the PhOH-NR, and it decreased with increasing clay loading. This observation indicated that the addition of clay affected the stress–strain behavior of NR and

Table III. Summary Data of Strain at Onset of Stress Upturn for PhOH-NR and PhOH-NRNCs Containing Different Clay Loading

Samples	Strain value (%)
PhOH-NR	495
PhOH-NRNC1	410
PhOH-NRNC3	300
PhOH-NRNC5	200
PhOH-NRNC10	125

lowered the strain at the onset of stress upturn, with increasing amount of clay.

Figure 5 shows the change of tensile strength and elongation at break of the PhOH-NR and PhOH-NRNCs filled with different clay loadings. Apparently, the tensile strength of the NR increased with an increase of clay content up to 5 phr clay, followed with a decrease of tensile strength at high clay content of 10 phr. Considering the TEM images shown in Figure 2, the PhOH-crosslinked NR/clay nanocomposite containing 10 phr clay (PhOH-NRNC10) showed that the dispersion of clay was relatively poor. It was well accepted that the good dispersion of filler in NR matrix prevented the formation of structural defects, as a result of aggregated filler, which weakened the NR network.[23–25] Thus, the poor dispersion of clay layer in the NR matrix filled with 10 phr clay caused a decrease of tensile strength. This result is also in accordance with the previous observation reported by the authors.[12–16,26] From Figure 5, it is also seen that the elongation at break decreased by adding clay and the decrease was more pronounced when the clay loading was increased. The reason for this decrease was because the deformation of NR matrix was greatly limited by an increase of clay loading.

WAXD Measurement

It is well established that NR can crystallize under stretching, which accounts for the obvious enhancement in the mechanical properties of NR.[4,5,27] Therefore, it is of great importance to

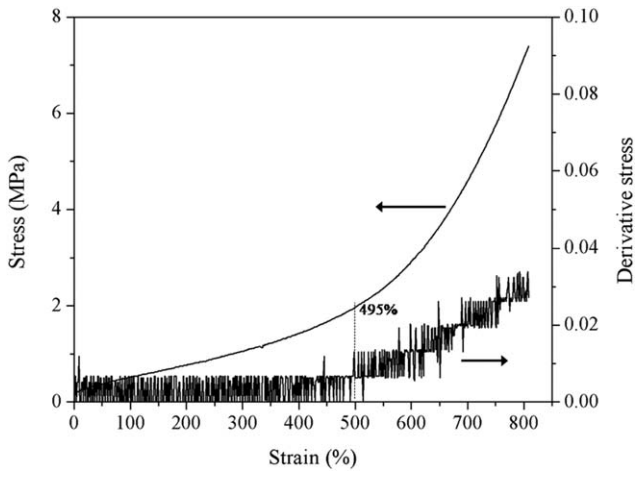

Figure 4. Coupled stress–strain curve and plot of derivative stress–strain of PhOH-NR.

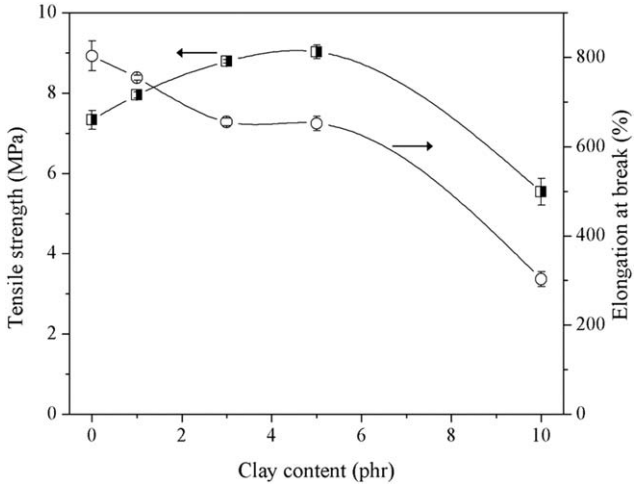

Figure 5. Change of tensile strength and elongation at break as a function of clay content of PhOH-NRNCs containing different clay loadings.

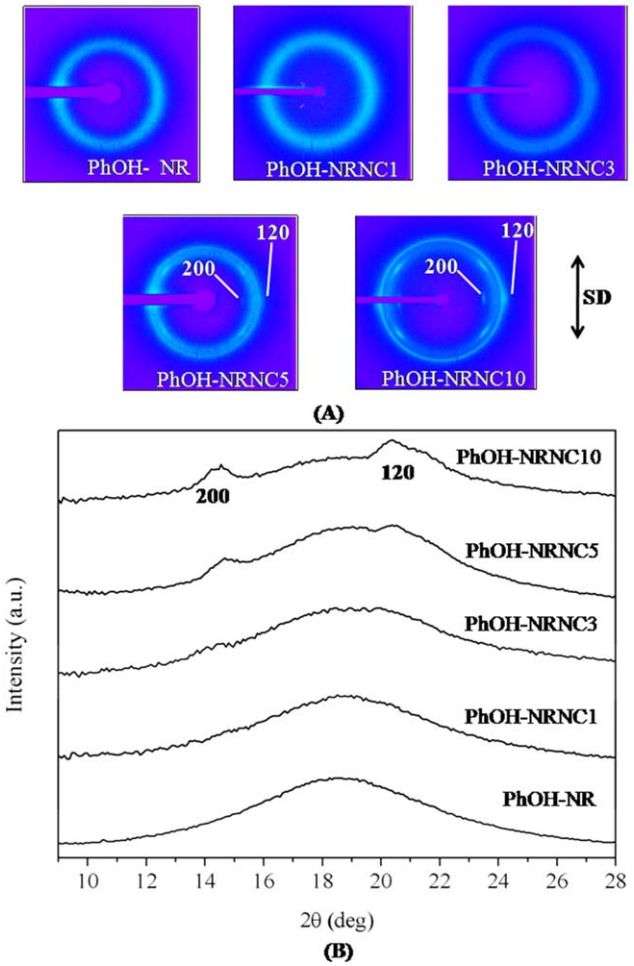

Figure 6. Coupled (A) 2D WAXD images and (B) linear WAXD patterns of PhOH-NR and PhOH-NRNCs containing different clay loadings measured at strain of 200%. [Color figure can be viewed in the online issue, which is available at wileyonlinelibrary.com.]

examine the effect of clay at various contents on the strain-induced crystallization of PhOH-NRNC. In order to monitor the evolution of strain-induced crystallization, the WAXD analysis of PhOH-NRNCs filled with 1–10 phr clay was carried out, and the results are shown in Figures 6–8.

Figure 6 shows 2D WAXD images coupled with their 1D WAXD patterns of PhOH-NR and PhOH-NRNCs containing various amounts of clay at the strain of 200%. From Figure 6(A), the 2D WAXD images of the PhOH-NRNCs containing 5 and 10 phr clay clearly show (200) and (120) reflection spots due to highly oriented crystallite in the NR. These two samples also show the crystal diffraction peaks, assigned to (200) and (120) plane reflection of the NR, at 2θ of about 14° and 20°, respectively [Figure 6(B)].[6] On the other hand, the WAXD images of the PhOH-NR and PhOH-NRNCs containing 1 and 3 phr clay did not show the reflection spots and their WAXD patterns still showed an amorphous halo at strain of 200%. For the neat NR crosslinked with 10 phr PhOH, it was found that the crystallization occurred at the strain level approximately about 300%, while the crystallization was developed at much lower strain of about 100% in the NR nanocomposite with 5

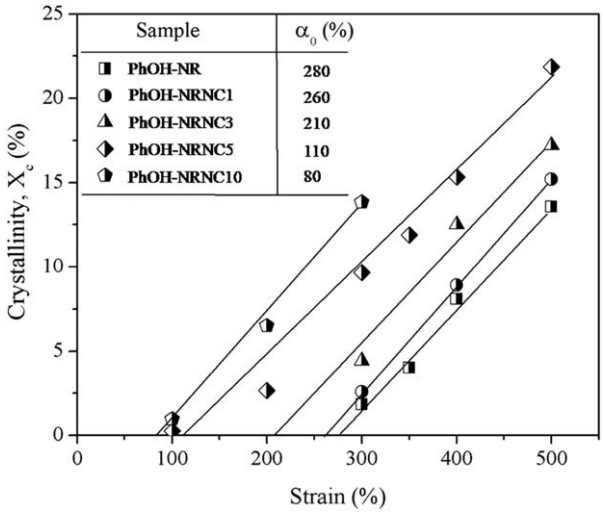

Figure 7. Change of crystallinity (X_c) as a function of strain of PhOH-NR and PhOH-NRNCs containing different clay loadings. Inserted table indicated onset strain for crystallization (α_0) of PhOH-NR and PhOH-NRNCs containing different clay loadings.

phr clay crosslinked with the same amount of PhOH because of faster NR chain alignment in the presence of clay.[11] It is also interesting to see that the intensities of crystalline peaks at the strain of 200% [Figure 6(B)] appeared to increase with increasing clay loading from 5 to 10 phr, indicating an increased NR chain alignment. At the same level of strain, however, the formation of crystallite in the NR matrix was not clearly observed in the NR nanocomposites with very low clay loading of 1–3 phr. These results suggested that a critical level of clay loading is required for strain-induced crystallization of NR at very low strain.

According to WAXD patterns of the PhOH-NR and PhOH-NRNCs at different levels of strain, the degree of crystallinity (X_c) could be determined from the intensities of the (200) and (120) plane diffraction peaks.[11,28] Figure 7 shows the change of X_c as a function of strain. The PhOH-NR and PhOH-NRNCs

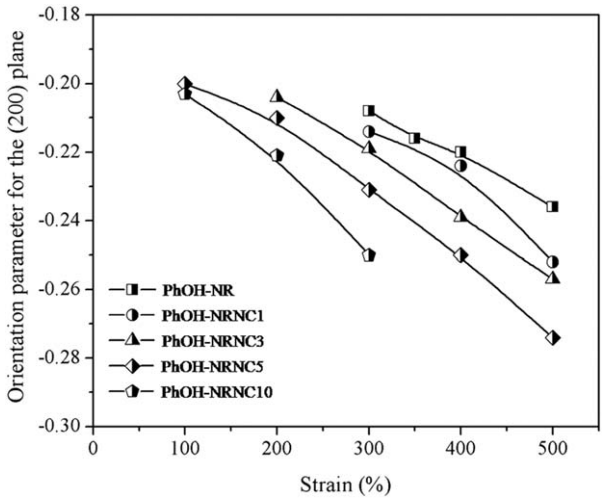

Figure 8. Change of orientation parameter (OP) as a function of strain of PhOH-NR and PhOH-NRNCs containing different clay loadings.

showed an increase of X_c with increasing applied strain because of strain-induced crystallization of the NR matrix.[11] At a given strain, the values of X_c increased with increasing clay loading. However, the maximum X_c was attained at 5 phr clay loading. Furthermore, it is seen that the onset strain of strain-induced crystallization (α_0), determined by the interception of the linear regression lines (solid lines in Figure 7) in the plot of crystallinity versus strain, decreased with increasing clay loading. The calculated α_0 values was about 280% for the PhOH-NR, and about 260%, 210%, 110% and 80% for the PhOH-NRNCs containing 1, 3, 5, and 10 phr clay, respectively. This trend is consistent with the observed change of strain at the onset of stress upturn as previously reported in Figure 3.

Figure 8 shows the orientation parameter (OP) of the PhOH-NR and PhOH-NRNCs with various clay loadings during stretching. The OP values of the crystal component in the PhOH-NR and PhOH-NRNCs at different strains obtained from azimutual scanning of the equatorial (200) reflection was estimated by using the Hermann orientation parameter, f,[29] as shown in the following equations,

$$f = \frac{3(\cos^2\theta) - 1}{2} \quad (1)$$

$$(\cos^2\theta) = \frac{\int_0^{\pi/2} I_c(\theta)\cos^2\theta \sin\theta d\theta}{\int_0^{\pi/2} I_c(0)\sin 0 d0} \quad (2)$$

where θ is the azimuthal angle from the stretching direction and $I_c(0)$ is the diffraction intensity of crystal component at 0. $I_c(\theta)$ was obtained by subtracting the minimum scattering intensity in the azimuthal scattering profile as the scattering intensity of the amorphous component from the original WAXD intensity.[30,31] The absolute values of OP in the PhOH-NR and PhOH-NRNCs increased with increasing strain, suggesting that the orientation of NR chain increased as the applied strain was increased. The absolute OP values of the PhOH-NRNCs were greater than that of the PhOH-NR at any given strain, and they increased upon increased incorporated clay. This indicated that the orientation of the NR chains in stretching direction was enhanced by adding more clay to the NR matrix. These results are in accordance with the increased crystallinity of the NR with increasing clay loading and applied strain as already shown in Figure 7.

On the basis of the mechanism of strain-induced crystallization for the PhOH-crosslinked NR/clay nanocomposite proposed by Masa *et al.*,[11] the strain-induced crystallization of NR was described by early crystallization of stretched NR chains due to clay orientation parallel to stretching direction at lower strain region (< 300%), followed by collaborative strain-induced crystallization of NR chains in the presence of dispersed clay and crosslinked points at high strain level (>300%). In this process, it was believed that the clay layers were interacted with NR chains through the strong specific interaction between PhOH functionalized NR and clay and intercalation of NR chains. Based on a verification by FTIR spectroscopy of chemical structure for the different samples (i.e., Na-MMT, PhOH, NR, PhOH-NR, PhOH-UNRNC, and PhOH-NRNC), which will be reported and discussed in the next section, the FTIR observation indicated that the chemical linkage at the interface between NR and clay was formed in the PhOH-crosslinked NR/clay nanocomposite (PhOH-NRNC). Thus, when the PhOH-crosslinked NR/clay nanocomposites (PhOH-NRNCs) were uniaxially stretched, the clay was rotated and aligned along the stretching direction. The interfacial interaction at the interface between NR and clay would constrain the NR chain mobility, thereby causing the chains easily stretched as the clay was rotated. This induces high stress concentration in the NR matrix at around the surface of clay. By this way, the clay having strong adhesion with NR could induce orientation and alignment of NR, and resulted in an early onset of the strain-induced crystallization of NR. Therefore, the increase of the clay loading increased numbers of NR chain restricted in mobility so that the onset strain for strain-induced crystallization of the PhOH-NRNCs was decreased and the degree of crystallinity was enhanced as shown in Figure 7. As a result, the early strain at the onset of stress upturn and improvement of tensile stress of the PhOH-NRNCs with increasing clay loading was obtained as previously shown in Figure 3.

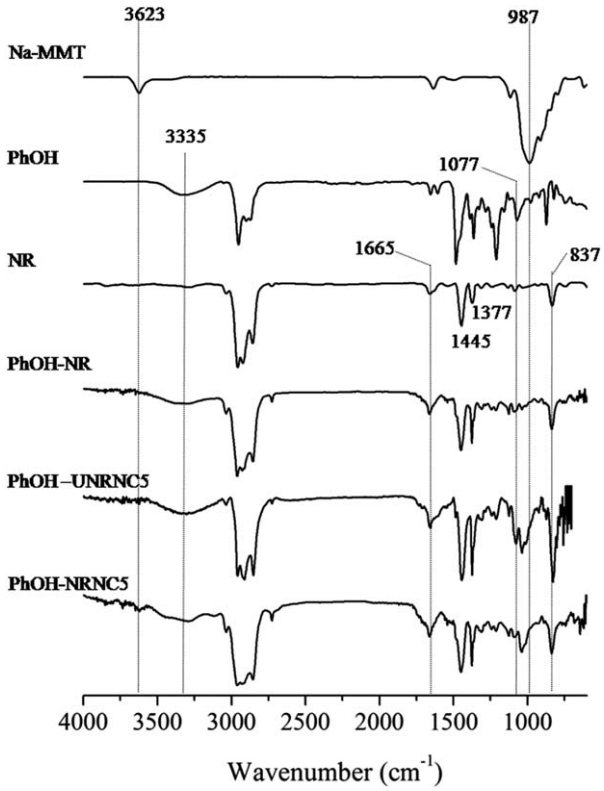

Figure 9. FTIR spectra in a range of 700–4000 cm^{-1} of Na-MMT, PhOH, NR, PhOH-NR, PhOH-UNRNC5, and PhOH-NRNC5.

FTIR Study

Figure 9 compares the representative FTIR spectra in the wave number range of 700–4000 cm^{-1} for the Na-MMT, PhOH, NR, PhOH-NR, and PhOH-NRNC5. Since, the compositions of PhOH-crosslinked NR/clay nanocomposites were kept the same, except for the clay loading, therefore the PhOH-crosslinked NR/

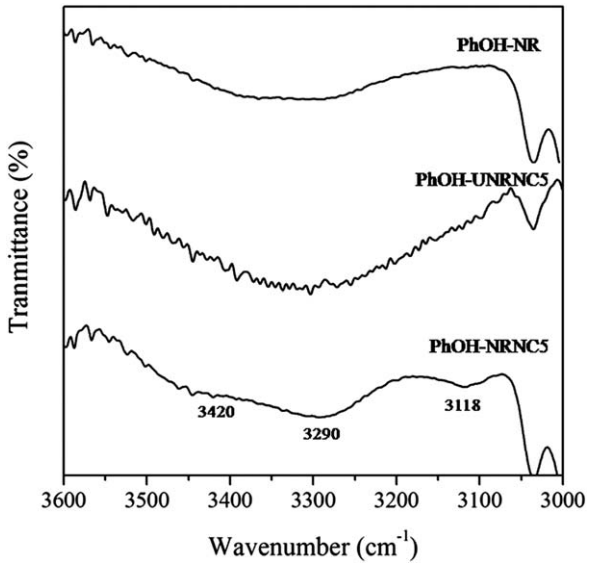

Figure 10. FTIR spectra in a range of 3000–3600 cm^{-1} for PhOH-NR, PhOH-UNRNC5, and PhOH-NRNC5.

clay nanocomposite containing 5 phr clay (PhOH-NRNC5) was chosen for comparison. The FTIR spectrum of NR/clay compound containing PhOH and 5 phr clay (PhOH-UNRNC5) was also included in Figure 9. The PhOH-UNRNC5 was prepared by mixing NR, clay, and PhOH at rotor speed of 140 rpm and temperature of 100°C for 20 min in order to eliminate the effect of crosslinking reaction of PhOH in the nanocomposite. For the Na-MMT, a sharp peak at 3623 cm^{-1} was assigned to the —OH stretching of silanol group (Si—OH) on the surface of clay[18,32] and the broad and intense peak centered at around 987 cm^{-1} was due to the vibration of Si—O bond in the silanol group (Si—OH) of clay.[33] The characteristic absorbance bands of the typical FTIR spectrum for the crosslinking agent (PhOH) appeared at 3335 cm^{-1} and 1077 cm^{-1}, which were assigned to the hydrogen bonded —OH vibration and C—O bond of phenolic resin, respectively.[34] The infrared spectrum of the NR showed the characteristic peaks at around 1665, 1445, 1377, and 837 cm^{-1}, which were associated with stretching vibration of C=C bond, bending vibration of CH_2 and CH_3 groups and out of plane deformation of =C—H group, respectively.[35–37] Upon crosslinking of NR with PhOH, the broad peak centered at 3324 cm^{-1} in the region of 3300–3600 cm^{-1} appeared in the FTIR spectrum of the PhOH-NR. It was more likely that the peak at 3324 cm^{-1} in the PhOH-NR sample was due to the presence of unreacted PhOH. In the PhOH-UNRNC5 (uncrosslinked nanocomposite), the spectrum showed corresponding peaks for the Na-MMT, PhOH, and NR. However, a remarkable change was found in the spectrum of the PhOH-NRNC5 by comparing with that of the PhOH-UNRNC5 and the peak positions were different to those of the Na-MMT, PhOH and PhOH-NR. To clarify the change of these bands in the nanocomposite due to crosslinking of NR/clay compound with phenolic resin, the spectra of the PhOH-NRNC5 in a limited region of 3600–3000 cm^{-1} and 800–1200 cm^{-1} are compared with those of the PhOH-NR and PhOH-UNRNC5 as shown in Figures 10 and 11, respectively.

Figure 10 shows FTIR spectra in a range of 3000–3600 cm^{-1} for the hydrogen bonded —OH groups of the PhOH in three different samples. There appeared a peak at 3420 cm^{-1} as a shoulder to a broad peak at 3290 cm^{-1} and another shoulder peak at 3118 cm^{-1} in the PhOH-NRNC5, while only single broad peak was seen in the PhOH-NR and PhOH-UNRNC5. This observation suggested that the —OH groups present in the PhOH-NRNC5 had different chemical environments when compared with those of PhOH-NR and PhOH-UNRNC5.

Figure 11 shows FTIR spectra in a range of 800–1200 cm^{-1} for the PhOH-NR, PhOH-UNRNC5, and PhOH-NRNC5. The spectrum of virgin clay was also included in this figure. On comparing with the PhOH-UNRNC5 and PhOH-NRNC5, it is clear that the peak at around 987 cm^{-1} presenting in the Na-MMT disappeared after the NR/clay compound was crosslinked with PhOH. In addition, the peak at about 1077 cm^{-1} which was due to C—O stretching in phenolic resin for the uncrosslinked NR/clay compound (PhOH-UNRNC5) was shifted to 1084 cm^{-1} by crosslinking. The leftward shift was also observed in the PhOH-NR. This suggested the change in local structure of C—O groups induced by crosslinking reaction for the NR with and without clay. Regarding the above observation, a change in chemical environment of specific functional groups of phenolic resin coupled with the absence of silanol groups of the clay in the PHOH-NRNC5

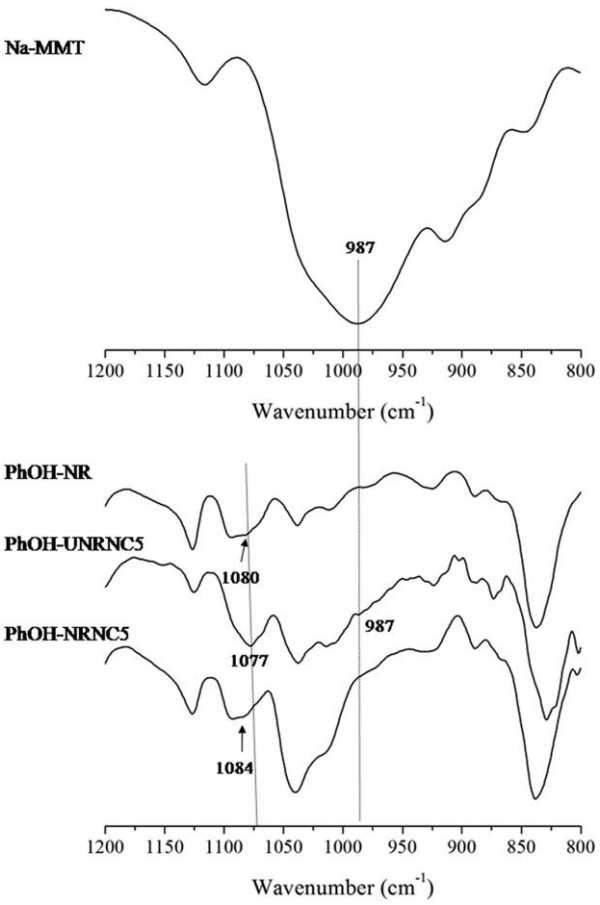

Figure 11. FTIR spectra in a range of 800–1200 cm^{-1} for Na-MMT and PhOH-NR, PhOH-UNRNC5, and PhOH-NRNC5.

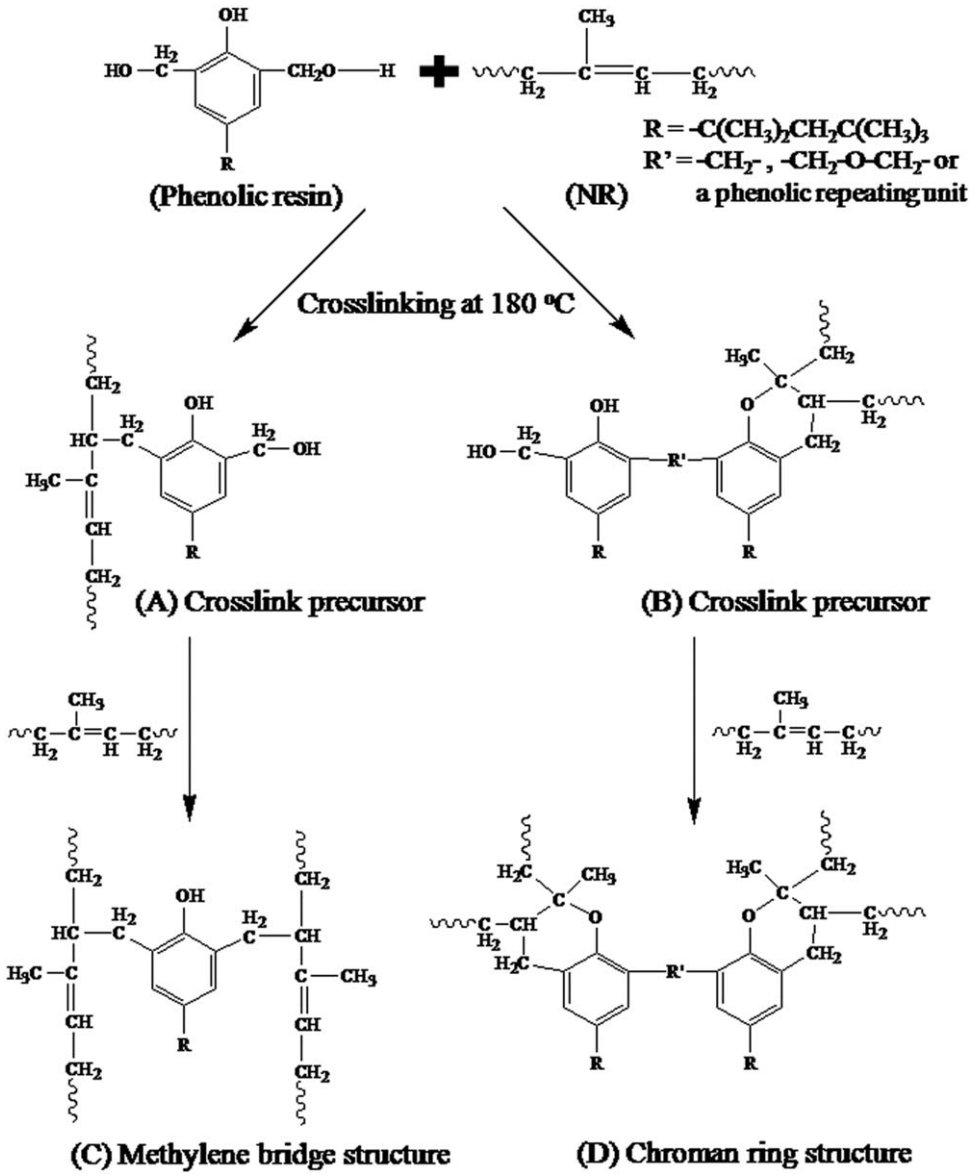

Figure 12. Crosslinking reaction between PhOH and NR.

proved that the clay had undergone chemical interaction with phenolic resin during chemical crosslinking process of NR. During heating at 180°C, the PhOH, having at least 1 aromatic ring/molecule, interacted with NR molecule to give precursor products with an unsaturated methylene bridge structure [Figure 12(A)] and/or a saturated chroman ring [Figure 12(B)]. The crosslink precursors then attached to another NR molecule to yield crosslinked products [Figure 12 (C,D)].[38,39] In the presence of clay, the OH group of methylol (—CH_2OH) group in the crosslinked precursor (PhOH functionalized NR) could chemically react with the OH group of silanol on the edge of clay surface. As a result, a strong bonding or adhesion existed between clay filler and NR matrix through PhOH bridges during crosslinking reaction using PhOH as shown in Figure 13.

According to the results obtained in this study, the mechanistic model[11] proposed to describe the strain-induced crystallization of PhOH-crosslinked NR/clay nanocomposite has been further refined with the concept of adhesion at NR and clay interface, which is shown in Figure 14. In the modified model, when the clay was rotated and aligned along the stretching direction, the strong adhesion between NR and clay via chemical reaction as discussed previously and intercalation of NR into clay layer would effectively allow for the chain orientation and alignment of NR chain for crystallization during tensile deformation, leading to early onset strain-induced crystallization and enhancement of crystallinity at low strain (< 300%). Later (> 300%), the crystallization induced from conventional crosslink point in the NR took part in crystallization process, in addition to the crystallization enhanced by dispersed clay (collaboration crystallization). Finally, a drastic increase of crystallinity and tensile stress was observed. Furthermore, the results showed that the PhOH did not only act as curative agent for crosslinking NR, but also worked as coupling agent at the interface between NR

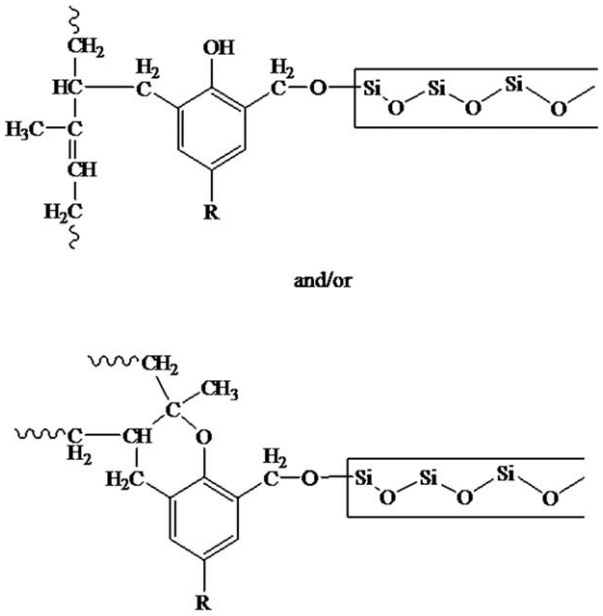

Figure 13. Proposed phenolic bridge formed between NR and clay.

and pristine clay in the NR/clay nanocomposite. To our best knowledge, this is the first report for enhanced interfacial adhesion of NR and pristine clay through the use of PhOH curative agent in NR/clay nanocomposites.

CONCLUSION

NR/pristine clay nanocomposites were prepared through latex compounding method. The nanocomposites were then crosslinked by using phenolic resin. The Influence of clay loading (1, 3, 5, and 10 phr) on mechanical properties and strain-induced crystallization of NR were studied. The PhOH-crosslinked neat NR was prepared for comparison. XRD patterns indicated the intercalation of NR chain into silicate layers. TEM images showed that the degree of dispersion was restricted at the high clay loading of 10 phr. Addition of clay resulted in an enhancement of stress upturn during stretching. The highest tensile strength of PhOH-crosslinked NR/clay nanocomposites was attained at 5 phr clay. Increasing the clay addition decreased an onset strain of strain-induced crystallization and enhanced crystallization of NR. FTIR observation indicated the formation of strong chemical bond at interface between NR and clay due to

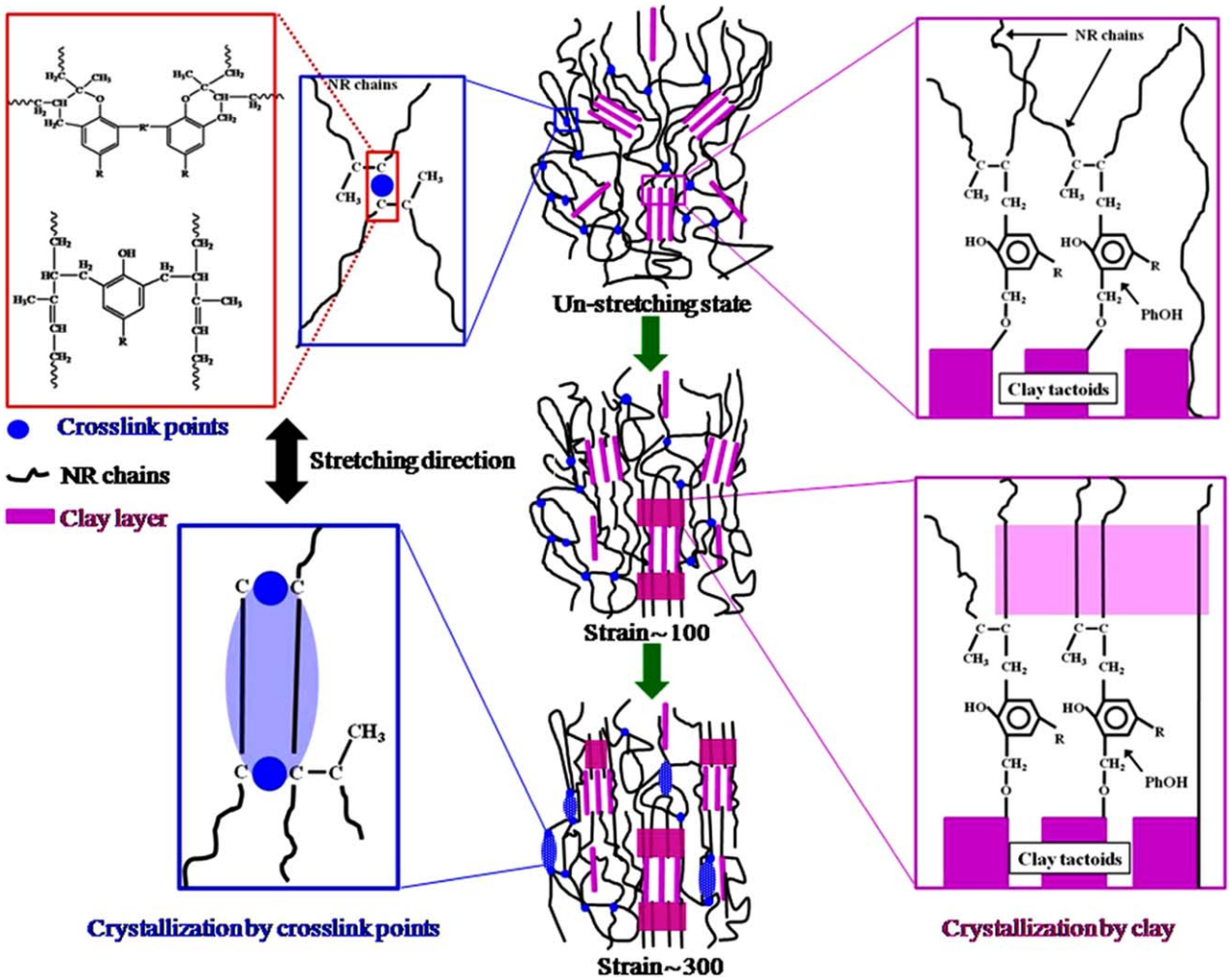

Figure 14. Proposed model for strain-induced crystallization mechanism of PhOH-crosslinked NR/clay nanocomposite in the presence of phenolic bridge and the intercalated NR chain during tensile stretching. [Color figure can be viewed in the online issue, which is available at wileyonlinelibrary.com.]

the specific reaction of NR, PhOH, and clay during crosslinking process. The strong adhesion by both chemical reaction and intercalation of NR facilitated the orientation and alignment of NR chains, leading to the early development of strain-induced crystallization and the increase of crystallinity, thus, providing a great improvement of mechanical property. Furthermore, the results present in this study suggested that the PhOH did not only act as curative agent by inducing crosslinking of NR, but it also worked as coupling agent by promoting interfacial interaction between NR and clay in the NR/clay nanocomposites.

ACKNOWLEDGMENTS

Authors gratefully acknowledge financial support from the Thailand Research Fund through the Royal Golden Jubilee Ph.D. Program (Grant No. PHD/0052/2554). Also a financial support from Graduate School, Prince of Songkla University, Thailand to the first author is gratefully acknowledged.

REFERENCES

1. Roberts, A. D. Natural Rubber Science and Technology; Oxford University Press: New York, **1988**.
2. Noordermeer, J. W. M. *Macromol. Symp.* **1998**, *127*, 131.
3. Thomas, S.; Stephen, R. Rubber Nanocomposites: Preparation, Properties and Applications; Wiley: Singapore: **2010**.
4. Toki, S.; Hsiao, B. S. *Macromolecules* **2003**, *36*, 5915.
5. Trabelsi, S.; Albouy, P. A.; Rault, J. *Macromolecules* **2003**, *36*, 7624.
6. Toki, S.; Sics, I.; Ran, S.; Liu, L.; Hsiao, B. S.; Murakami, S.; Senoo, K.; Kohjiya, S. *Macromolecules* **2002**, *35*, 6578.
7. Carretero-Gonzalez, J.; Verdejo, R.; Toki, S.; Hsiao, B. S.; Giannelis, E. P.; Lopez-Manchado, M. A. *Macromolecules* **2008**, *41*, 2295.
8. Carretero-Gonzalez, J.; Retsos, H.; Verdejo, R.; Toki, S.; Hsiao, B. S.; Giannelis, E. P.; Lopez-Manchado, M. A. *Macromolecules* **2008**, *41*, 6763.
9. Nie, Y.; Huang, G.; Qu, L.; Wang, X.; Weng, G.; Wu, J. *Polymer* **2011**, *52*, 3234.
10. Nie, Y.; Qu, L.; Huang, G.; Wang, X.; Weng, G.; Wu, J. *J. Appl. Polym. Sci.* **2014**, *131*, 40324.
11. Masa, A.; Iimori, S.; Saito, R.; Saito, H.; Sakai, T.; Kaesaman, A.; Lopattananon, N. *J. Appl. Polym. Sci.* **2015**, *132*, 42580.
12. Wang, Y.; Zhang, H.; Wu, Y.; Yang, J.; Zhang, L. *Eur. Polym. J.* **2005**, *41*, 2776.
13. Wang, Y.; Zhang, H.; Wu, Y.; Yang, J.; Zhang, L. *J. Appl. Polym. Sci.* **2005**, *96*, 318.
14. Qu, L.; Huang, G.; Liu, Z.; Zhang, P.; Weng, G.; Nie, Y. *Acta Mater.* **2009**, *57*, 5053.
15. Nie, Y.; Qu, L.; Huang, G.; Wang, B.; Weng, G.; Wu, J. *Polym. Adv. Technol.* **2012**, *23*, 85.
16. Fu, X.; Huang, G.; Xie, Z.; Xing, W. *RSC Adv.* **2015**, *5*, 25171.
17. Mittal, V. *Materials* **2009**, *2*, 992.
18. Chen, G. X.; Kim, H. S.; Shim, J. H.; Yoon, J. S. *Macromolecules* **2005**, *38*, 3738.
19. Morgan, A. B.; Gilman, J. W. *J Appl. Polym. Sci.* **2003**, *87*, 1329.
20. Luo, Z. P.; Koo, J. H. *Polymer* **2008**, *49*, 1841.
21. Navarchian, A. H.; Majdzadeh-Ardakani, K. *J. Appl. Polym. Sci.* **2009**, *114*, 531.
22. Karino, T.; Ikeda, Y.; Yasuda, Y.; Kohjiya, S.; Shibayama, M. *Biomacromolecules* **2007**, *8*, 693.
23. Lopattananon, N.; Jitkalong, D.; Seadan, M. *J. Appl. Polym. Sci.* **2011**, *120*, 3242.
24. Tan, J.; Wang, X.; Luo, Y.; Jia, D. *Mater. Des.* **2012**, *34*, 825.
25. Stumpe, N. A.; Railsback, H. E. *Rubber World* **1964**, *151*, 41.
26. Mathew, S.; Varghese, S. *J. Rubber Res.* **2005**, *8*, 1.
27. Jiang, H. X.; Ni, Q. Q.; Natsuki, T. *Polym. Compos.* **2010**, *31*, 1099.
28. Hernandez, M.; Lopez-Manchado, M. A.; Sanz, A.; Nogales, A.; Ezquerra, T. A. *Macromolecules* **2011**, *44*, 6574.
29. Roe, R.-J. Methods of X-Ray and Neutron Scattering in Polymer Science; Oxford University Press: New York, **2000**.
30. Osaka, N.; Kato, M.; Saito, H. *J. Appl. Polym. Sci.* **2013**, *129*, 3396.
31. Ran, S.; Zong, X.; Fang, D.; Hsiao, B. S.; Chu, B.; Phillips, R. A. *Macromolecules* **2001**, *34*, 2569.
32. Kim, E. S.; Shim, J. H.; Woo, J. Y.; Yoo, K. S.; Yoon, J. S. *J. Appl. Polym. Sci.* **2010**, *117*, 809.
33. Madejová, J. *Vib. Spectrosc.* **2003**, *31*, 1.
34. Choi, S. S.; Cho, G. *J. Appl. Polym. Sci.* **1998**, *68*, 1811.
35. Arjunan, V.; Subramanian, S.; Mohan, S. *Spectrochim. Acta A* **2001**, *57*, 2547.
36. Santos, K. A. M.; Suarez, P. A. Z.; Rubim, J. C. *Polym. Degrad. Stab.* **2005**, *90*, 34.
37. Pathak, A.; Saxena, V.; Tandon, P.; Gupta, V. D. *Polymer* **2006**, *47*, 5154.
38. Lattimer, R. P.; Kinsey, R. A.; Layer, R. W. *Rubber Chem. Technol.* **1989**, *62*, 107.
39. Duin, M.; Souphanthong, A. *Rubber Chem. Technol.* **1995**, *68*, 717.